APPLICATION OF DISCONTINUOUS GALERKIN METHOD FOR EXTERNAL AERODYNAMIC FLOWS

A.V.Wolkov*, S.V.Lyapunov*, Ch.Hirsch**
* TsAGI, Moscow,Russia, ** NUMECA Int. Brussels, Belgium

Abstract

The Discontinuous Galerkin method (DGM) is based on a generalization of the finite-element approach showing many advantages in comparison with the finite-volume method (FVM) that at present is widely used in CFD.

The current objectives of aerodynamic design require more accurate calculations of aerodynamic characteristics of different aircraft elements, as well as for the full aircraft. The standard computational schemes based on second order finite-volume approach require extremely fine meshes and consequently involve considerable computational resources.

Two ways to reduce required computer resources can be considered. The first one requires the application of highly anisotropic adaptive meshes and the second one is related to high order accurate approximation schemes. As it is shown in previous investigations [1], DGM offers higher accuracy in comparison with FVM on highly anisotropic meshes, even with the same polynomial order for solution reconstruction. Calculation with high order accuracy in DGM is performed on local stencils that provide easier realization of the high accurate calculations and does not need to choose appropriate stencil. Moreover, DGM makes it possible to perform adaptation of polynomial order to peculiarities of a flow that provides wide perspective of their future usage.

1 Introduction

Improvement of quality and reduction of design time of new aircraft connected with perfection of numerical methods of aerodynamic characteristics prediction. A new level of aircraft design is related to application of the full Navier-Stokes or Reynolds equations. In the last one and a half decade a plenty of approaches to the solution of these equations has been developed. The most successful numerical schemes realized in well-known commercial packages (FLUENT, CFX, STAR-CD, NUMECA), have received a wide circulation and are rather successfully used for solution of many applied problems. Aerodynamic design of aircraft configurations with these schemes demand significant computer and human resources that leads to appreciable rise in cost of calculation results and prevents wide application of these methods for practical design problems.

As a rule modern numerical schemes are based on a finite-volume (FVM) or less often finite-difference (FDM) methods of the second order of accuracy. It is known that increase of the order of accuracy of numerical schemes allows one to reduce the involved computing resources. Other potential opportunity of economy can be connected with use anisotropic adaptive meshes. At present meshes with isotropic adaptation of the cells are used in some industrial codes but they do not give essential profit. Anisotropic meshes (with cells stretched in the some direction) essentially more economical but approximation by modern approaches of the conservations laws on such meshes are very problematic. FVM provides good results only on isotropic uniform (or almost uniform) meshes. Increase of the accuracy order of FVM leads to necessity of expansion of approximation stencil and to the requirement of improvement of mesh quality. Thus one of ways to provide high efficiency of numerical schemes is connected with use of

high order schemes that permits one to perform calculations on anisotropic adaptive meshes.

The alternative to FVM and FDM is finite element method (FEM). Generally speaking FEM demands greater number of arithmetic operations in comparison with FVM. However, it turned out that this method gives more ample opportunities for reduction of the computer resources necessary for solution of industrial problems. These opportunities can be realized by means of use of not only anisotropic mesh adaptation but also adaptation of the local accuracy order of the scheme to features of the flow. Numerical schemes based on FEM show the best results on the stretched deformed meshes i.e. meshes with adaptation of cells to anisotropic features of the flow.

One of the most perspective approaches to accurate approximation on the basis of FEM is Discontinuous Galerkin Method (DGM). Last years this method attracts many researchers due to its generality, flexibility and reliable theoretical basis. At first the method has been proposed in [2] and first theoretical analysis has been given in [3]. The numerical solution of 2-D Euler and Navier-Stokes equations on unstructured triangular meshes for the first time was presented in [4, 5]. The most general theoretical description of DGM with numerous solution examples of 1-D and 2-D problems is given in [6, 7].

Discontinuous Galerkin approach has many attractive features:
o Opportunity of approximation on meshes with cells of arbitrary shapes, including cells with hanging nodes;
o Smaller sensitivity to mesh quality in comparison with FDM and FVM that provides an opportunity to use the method on adaptive meshes;
o The high order of accuracy is reached with use of a compact stencil that simplifies the organization of parallel calculations;
o In different cells of a mesh different basic functions can be used that provides an opportunity of basis functions adaptation to local features of the flow.
o Opportunity of achievement of «superconvergence» with order O(h^{2K+1}) for

value of objective function (K is the maximal polynomial order).

In the present paper some basic advantages of the DGM are shown on solution examples of external aerodynamics problems. In particular the following three test cases were considered:
1. An example of polynomial adaptation to flow properties for a transonic flow around a single airfoil;
2. Demonstration of DGM calculations on adapted meshes around a multi-element airfoil;
3. An example of DGM calculations for 3-D flow about a wing-body configuration DLR F-4. The calculated results and required computer resources are compared with a standard FV method.

2 Governing Equations

Consider the system of Navier-Stokes equations in the conservative form:

$$\frac{\partial \mathbf{U}(t,\mathbf{x})}{\partial t} + \nabla \cdot (\mathbf{F} - \mathbf{F}_v) = \mathbf{S} . \qquad (1)$$

Source term $\mathbf{S}$ is added to right hand side of this system for implementation of turbulence model. In our test cases Spallart-Almaras turbulence model was used.

Below we shall obtain numerical approximation of the given system of the equations by Discontinuous Galerkin method. The solution in each cell is stored in primitive variables $\mathbf{Q} = (\rho, u, v, w, p)$ thus the system (1) can be rewritten as follows:

$$\mathbf{\Gamma}\frac{\partial \mathbf{Q}}{\partial t} + \nabla \cdot \left(\mathbf{F}(\mathbf{U}(\mathbf{Q})) - \mathbf{F}_v(\mathbf{U}(\mathbf{Q}),\nabla \mathbf{U}) \right) - \mathbf{S} = 0 , \quad (2)$$

where a matrix $\mathbf{\Gamma} = \left(\dfrac{\partial \mathbf{U}}{\partial \mathbf{Q}} \right)$ is a transformation Jacobian from conservative variables to primitive ones. In each cell of a mesh local polynomial basis functions $\varphi_j(\mathbf{x})$ are defined, and linear combination of them defines the solution in a cell:

$$\mathbf{Q}(t,\mathbf{x}) = \sum_{j=1}^{K_f} \mathbf{u}_j(t)\varphi_j(\mathbf{x}) . \qquad (3)$$

Here $\mathbf{u}_j(t)$ is a vector of decomposition coefficients which should be defined during

solution; K_f – the number of different basis functions in a cell. Size K_f it is connected with the maximal degree of a basis polynomial K in 2-D case:

$$K_f(K) = \frac{(K+1)(K+2)}{2},$$

or in 3-D case:

$$K_f(K) = \frac{(K+1)(K+2)(K+3)}{6}. \qquad (4)$$

System of discritization equations for coefficients $\mathbf{u}_j(t)$ from (3) is obtained in accordance with standard procedure of finite element Galerkin approach in which orthogonality of residual (the left part of system (2)) to each basis function is required. The requirement of orthogonality is formulated through a condition of equality to zero of integral from product of the solved equations by each of basis function $\varphi_j(\mathbf{x})$ ($i=1,\ldots, K_f$). After integration by parts we have:

$$\frac{\partial}{\partial t} \int_\Omega \varphi_i\, \mathbf{\Gamma Q} d\Omega = -\oint_\Sigma \varphi_i\left(\mathbf{F} - \mathbf{F}_v\right)\cdot\mathbf{n}\,d\Sigma +$$
$$+ \int_\Omega \nabla\varphi_i\left(\mathbf{F} - \mathbf{F}_v\right)d\Omega + \int_\Omega \varphi_i \mathbf{S} d\Omega \qquad (5)$$

Here $d\Sigma$ – element of the area, $\mathbf{n} = \left(n_x, n_y, n_z\right)$ – normal to an element of the area, and $d\Omega$ – an element of a cell volume.

The equation (5) consists of volume integrals and surface integrals over boundaries of a cell. Values of dependable variables are discontinuous at interfaces of elements and rules of calculation of variables and fluxes at cell boundaries play the key role here.

As well as in a method of finite volume in DGM the inviscid flow at interfaces between different cells is defined as a result of the solution of Riemann problem. In the present realization we used Roe approach.

Viscous terms are defined through gradient of primitive variables $\mathbf{F}_v = \mathbf{F}_v\left(\mathbf{Q}, \nabla\mathbf{Q}\right)$, where $\nabla\mathbf{Q} = \left(\dfrac{\partial\mathbf{Q}}{\partial x}, \dfrac{\partial\mathbf{Q}}{\partial y}, \dfrac{\partial\mathbf{Q}}{\partial z}\right)$. Gradients of primitive variables can be found by direct differentiation of the expression (3). However such way of calculation of gradients cannot be used since it leads to absence of approximation [8].

Therefore in DGM the gradients of primitive variables also are represented in the form of a linear combination of basic functions for calculation of viscous terms:

$$\frac{\partial\mathbf{Q}}{\partial x_i}(t, \mathbf{x}) = \sum_{j=1}^{K_f} \mathbf{g}_{i,j}(t)\,\varphi_j(\mathbf{x})\,. \qquad (6)$$

Here $i=1$, 2 and 3 corresponds to x, y and z coordinates respectively. After multiplication of the equation (6) by test function and integration by parts we get the following system of the linear equations for decomposition coefficients $\mathbf{g}_{i,j}$:

$$\int_\Omega \sum_{j=1}^{K_f} \mathbf{g}_{i,j}\varphi_j\varphi_k d\Omega + \oint_\Sigma \varphi_k\mathbf{Q}\,n_i d\Sigma - \int_\Omega \frac{\partial\varphi_k}{\partial x_i}\mathbf{Q}d\Omega = 0\,,$$
$$k = 1,\ldots,K_f\,. \qquad (7)$$

Solution of the system (7) provides gradients of primitive variables (6) and enables one to calculate viscous terms in a cell.

In DGM both gradients of primitive variables and fluxes are discontinuous at cell boundaries. These values are required for calculation of surface integrals and they cannot be obtained by averaging. According to [6] for definition of the solution at the interface between cells are used different (left or right) cells for different ((5) or (7)) equations. Namely if calculation of viscous terms in (5) is based on values from the left cell $\mathbf{F}_v\big|_b = \mathbf{F}_v\left(\mathbf{Q}^L, \nabla\mathbf{Q}^L\right)$, than in the equation (7) for calculation of surface integrals the values of primitive variables should be taken from the right cell: $\mathbf{Q}\big|_b = \mathbf{Q}^R$. More advanced realization of viscous term approximation is presented in [9].

Finally a system of nonlinear equations for coefficients $\mathbf{u}_j(t)$ is expressed from system (2) under the assumption of a small variation of Jacobian $\mathbf{\Gamma}$ inside of a cell:

$$\frac{d\mathbf{u}_i}{dt} = \mathbf{\Gamma}^{-1}\mathbf{M}^{-1}\begin{bmatrix} -\oint_\Sigma \varphi_i\left(\mathbf{F} - \mathbf{F}_v\right)\mathbf{n}\,d\Sigma + \\ \int_\Omega \nabla\varphi_i\left(\mathbf{F} - \mathbf{F}_v\right)d\Omega + \\ \int_\Omega \varphi_i\, \mathbf{S}\, d\Omega \end{bmatrix}. \qquad (8)$$

Here **M** is a matrix that contains integrals of products of various combinations of basic functions.

For solution of the obtained system (8) for 2-D problems we used implicit approach, described in details in [10] and for 3-D cases the p-multigrid approach with local implicit solver is used [11].

3. Reduction of arithmetic operations

The system of the discretizied equations (8) consists of a set of surface integrals over a boundary of a control volume and control volume integrals. Correct definition of these integrals leads to reliable iterative convergence of the numerical scheme to the solution and finally defines accuracy of the obtained solution.

Generally speaking, application of DGM is possible on meshes with cells of arbitrary shapes. Thus one of the basic requirements is the opportunity of splitting of sides of a cell and its internal volume on elementary shapes, for example, a triangle and a quadrilateral or a tetrahedron and hexahedron. The following step consists in transformation of these shapes in canonical coordinates in which position of their nodes is strictly determined. The triangle and tetrahedron are transformed in canonical coordinates on the basis of simple linear transformation while transformation of a quadrilateral and hexahedron to a square and a cube demands application of nonlinear transformation that complicates subintegral function by presence of a nonlinear transformation Jacobian.

Integration over elementary shapes in canonical coordinates is carried out with use of Gauss quadrature rules which define integration as the sum of values of subintegral function in Gauss points with the certain weights. It is desirable that the choise of quadrature rules should provide accurate integration in (5) for the maximum polynomial order including transformation Jacobian under the integrals. However, in the present work quadrature rules with lower accuracy, than it is described above were used. Namely qudrature rules were exact for polynomials of degree $3 \cdot K$ when integrated

in canonical space. There are many of such kind of rules. Final selection of quadrature rule was based on the best satisfaction of the following requirements when integrated in the physical space:

$$\iiint\limits_{\Omega} k\, r^{k-1} \mathrm{d}\Omega - \oiint\limits_{\Sigma} r^k n_r \mathrm{d}\Sigma = 0\,, \quad r = \{x, y, z\}\,,$$

$$k = 1, 2, ..., 3 \cdot K\,,$$

where n_x, n_y, n_z – components of a normal to a boundary of an element. The given expression is the consequence of the divergence theorem. Note that control volumes in physical space have curved faces.

The number of Gauss points in quadrature rules basically defines total number of arithmetic operations of the method in general. The searching of rules with a minimum number of points for a given accuracy is a relevant mathematical problem and its solution allows one to reduce required CPU time. Optimization problem that was solved within the present work consisted in searching of optimum distribution of Gauss nodes on a surface of control volume and inside it. The points used for calculation of surface integrals can be involved for calculation of volume integral thus reducing a number of internal Gauss nodes. Code for searching of optimal distribution of the Gauss nodes was based on minimization of objective functional by quasi-Newton method. Positions of points inside a cube, their weights, and also weights for points at a cube sides are defined with the constraints that positions of these last points were fixed according to qudrature rules for surface integration. The sum of squares of differences between analytical and numerical values of all basis functions integral was taken as an objective function. The optimization procedure reduced this function to less than 10^{-22}. The performed optimization allowed to reduce the number of used internal points and to reduce the general estimated time by $15-20$ %.

Other possible approach to reduction of a number of arithmetic operations is based on analytical calculation of necessary integrals. For these purposes flux function is decomposed in a set of basic functions: $\mathbf{F}(\mathbf{U}) = \sum\limits_{j=1}^{M_f} \mathbf{f}_j\, \varphi_j$. Here M_f

– is the total number of decomposition

elements. M_f can be distinct from a given quantity of basic functions in an element K_f. In present work, the number of decomposition terms M_f was taken to be greater than the number of basic functions K_f in an element in accordance with the following rule $M_f = K_f (K+1)$ (see definition (4)). Such representation of fluxes allows one to express their integrals as the sum of integrals of simple polynomial expressions:

$$\iiint_\Omega \nabla\varphi_i \mathbf{F}(\mathbf{U}) d\Omega = \iiint_\Omega \nabla\varphi_i \mathbf{f}_j \ \varphi_j d\Omega = \mathbf{f}_j \iiint_\Omega \nabla\varphi_i \ \varphi_j d\Omega ,$$

$$\oiint_\Sigma \varphi_i \mathbf{F}(\mathbf{U}) \mathbf{n} \, d\Sigma = \oiint_\Sigma \varphi_i \mathbf{f}_j \ \varphi_j \mathbf{n} d\Sigma = \mathbf{f}_j \oiint_\Sigma \varphi_i \varphi_j \ \mathbf{n} \ d\Sigma .$$

Integrals from basis functions can be found analytically in advance. Such method named as quadrature free approach and was proposed in [12]. In the implemented DGM on unstructured hexahedral meshes application of quadrature free approach has appeared effective only at coarse multigrid levels where the basic goal for solver consists in reduction of a low-frequency error of the solution for a fine mesh. At the top multigrid level where the largest number of degrees of freedom is used, integration was carried out on the basis of quadrature approach.

4. Application of DGM to external problems

4.1 Solution with p-refinement for Airfoil Flow

As it was mentioned above, one of potential advantages of DGM is the opportunity of a variation of the order of accuracy of the scheme in different areas of the flow (variation of the polynomials order approximating the solution), and also adaptations of the scheme to the solution by means of variation of the order (p-refinement). Increase of the order of accuracy of the scheme will be the most effective in areas where the solution is smooth, but rapidly varying, for example, in boundary layers. As a first step in this direction the numerical solution of a problem for viscous turbulent flow about single airfoil RAE2822 is considered under conditions M=0.725, α=2.92°, Re=6.5·10^6 (Case-6) [13].

The boundary layer velocity profiles are presented in Figs. 1 a, 1 b and 1 c for three different sections A, B and C.
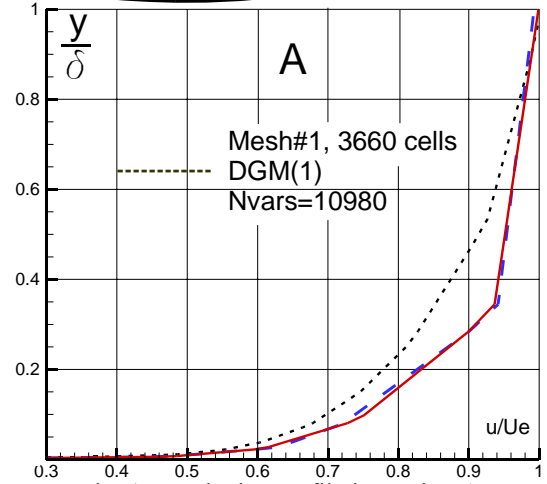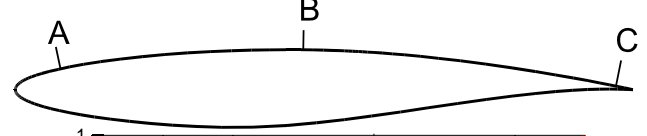

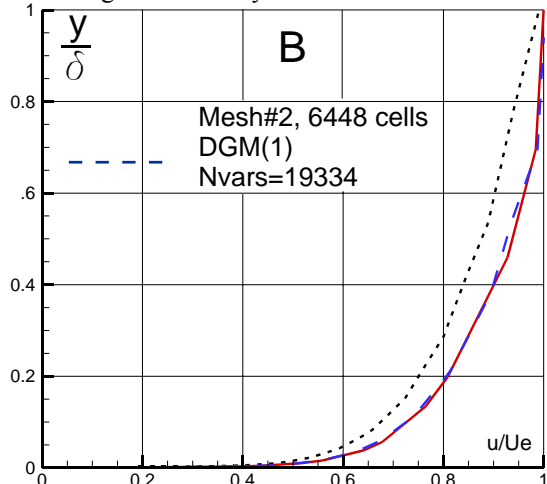Fig. 1 a. Velocity Profile in section A
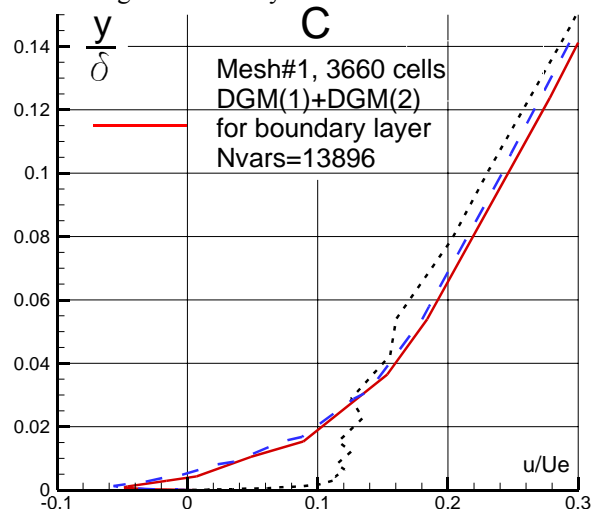
Fig. 1 b. Velocity Profile in section B

Fig. 1 c. Velocity Profile in section C

In each section three solutions are presented. Solution #1 is obtained on coarse mesh#1 (3660 cells) with second order DGM(K=1) scheme (10980 degrees of freedom). The accuracy of this solution is not good enough. The solution #2 is obtained on finer mesh#2 with 6448 cells using DGM(K=1) (19334 degrees of freedom). Numerous calculations on different meshes with larger number of cells showed that solution #2 is accurate enough. In other words the solution received on finer meshes, coincides with the solution on a mesh #2. The solution #3 is obtained on a coarse mesh#1 but in boundary layer region the third order DGM(K=2) scheme was used. The number of degrees of freedom in this case was 13869 that is less in comparison with solution #2. Nevertheless the calculated results and velocity profiles in particular are close to the solution #2. That is a good demonstration of the p-refinement efficiency application in the regions with smooth solution.

4.2 Calculation of the Flow Around Multielement Airfoil Using a Sequence of Adapted Unstructured Grids

Adapted grids make it possible to achieve an optimal distribution of the grid points. The first calculation is performed on a very coarse initial grid, which can be generated automatically. Then, in accordance with the solution, an adaptation procedure is performed that changes the position of some existing grid points and links between them and adds (or removes) some other points. The process solution–adaptation–solution is repeated until the change in the characteristics of the flow between iterations becomes less than a predefined small value. In the present work, we use the method of grid adaptation and the software implementing this method developed in [14]. The adaptation process is based on a heuristic error indicator that depends on a linear combination of the first- and second-order derivatives of the local Mach number along the edge. The grid is subdivided into macrocells that are split or refined in an isotropic manner. The points on the macrocell edges are distributed with account for the anisotropic properties of the flow.

The calculation of the flow around a three-element high-lift system of McDonnell Douglas Corporation (MDC) was performed using a sequence of adapted unstructured grids for M=0.2, Re=9×10^6, which corresponds to the experimental conditions [15]. The slat and flap settings of this configuration are presented in Table 1. Fragments of the adapted grid obtained after eight iterations of adaptation are shown in Figs. 2a, 2b, 2c for angle of attack 24 degrees.

Table-1. Slat and Flap Settings

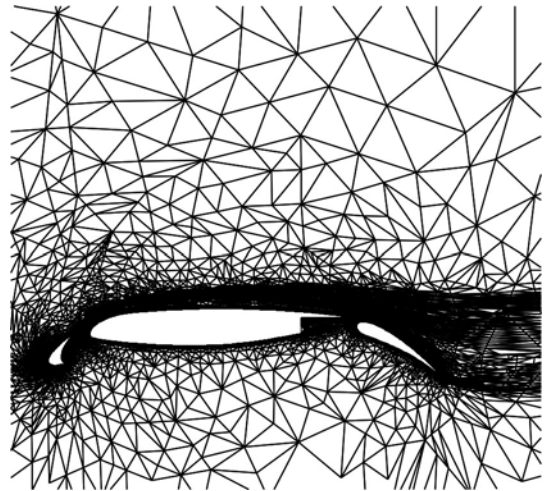|	Slat	Flap
Deflection	-30°	30°
Gap	2.95%	1.27%
Overhang	-2.5%	0.25%

Fig. 2 a. Fragment anisotropic adaptive mesh around three element airfoil
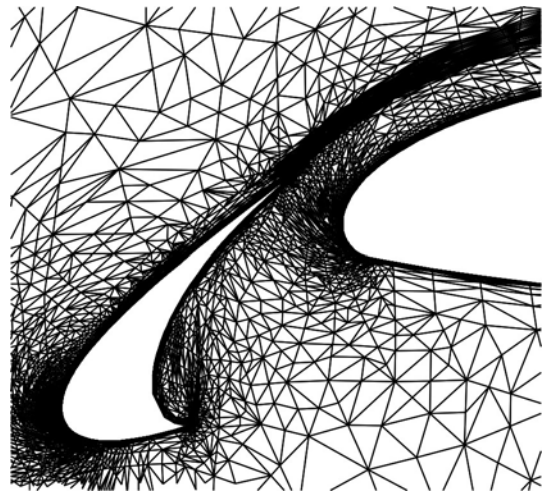

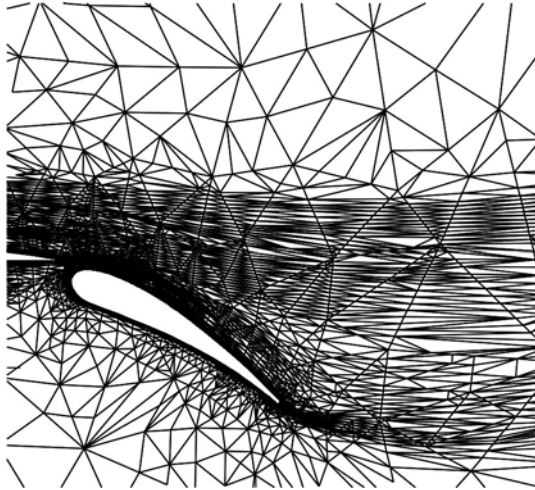Fig. 2 b. Fragment anisotropic adaptive mesh around slat of three element airfoil

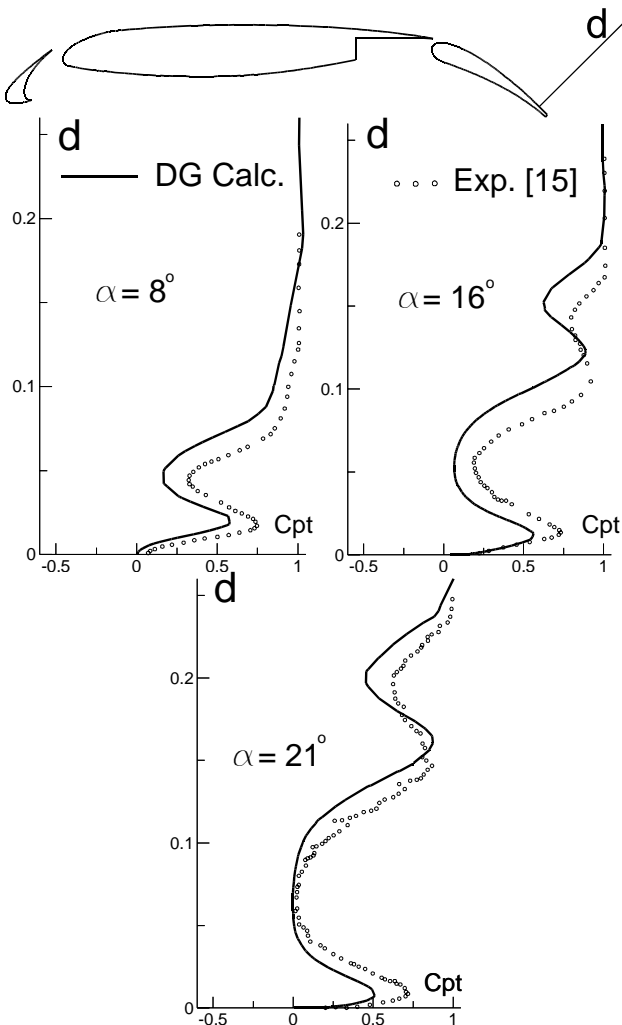Fig. 2 c. Fragment anisotropic adaptive mesh around flap of three element airfoil

attack $\alpha = 8°$, 16°, and 21° as compared to the experimental results. The comparison shows that the generated adapted grids provide a fairly accurate resolution of the wake formed by the forward elements of the high-lift system.

The lift force as a function of the angle of attack, which is of great practical importance, is illustrated in Fig. 4. It is seen that the calculation accurately predicts the critical angle of attack and the value of the maximum lift force.
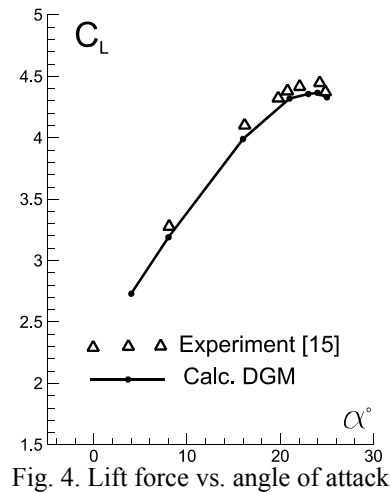

Fig. 4. Lift force vs. angle of attack

Fig.3. Profiles of the total pressure over the flap

Figs. 3a, 3b, 3c show the profiles of the total pressure coefficient $Cpt = \dfrac{2(p_0 - p_\infty)}{\rho_\infty u_\infty^2}$ in the wake over the flap (x/c = 0.975) at the angles of

Although the Mach number of the incoming flow is small, the flow around the configuration under examination is characterized by the existence of a short local supersonic zone that ends in a pressure shock on the upper surface of the slat. The use of adapted grids made it possible to resolve this important feature of the flow (see Fig. 5, which shows the distribution of the local Mach numbers near the leading edge of the slat of the three-element profile MDC, M = 0.2, $\alpha = 24°$ (the critical angle of attack), and Re $= 9 \cdot 10^6$.
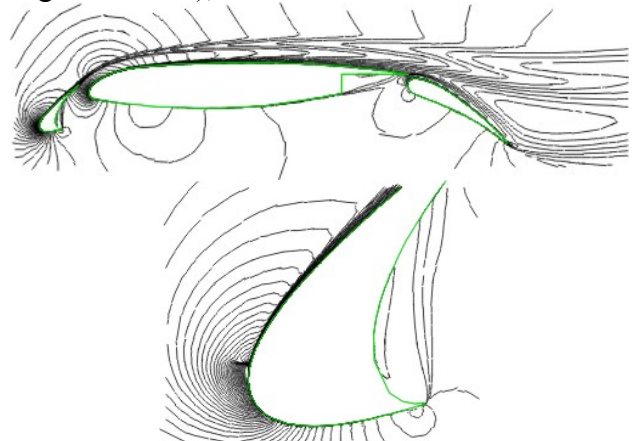

Fig.5 Distribution of the local Mach numbers near the slat

In current investigations the number of element in meshes that generated during adaptation procedures not exceed 30 000 elements. Our experience showed that results of similar quality can be obtained with using of the standard FVM on meshes with number of cells more than 100 000.

4.3 Turbulent 3D flow around a DLR-F4 wing-body configuration

Aircraft configuration «wing+body» DLR-F4 chosen as test model for AIAA CFD Drag Prediction Workshop (DPW) has been calculated by DGM(K=1) on a mesh containing 230 000 cells. The size of the mesh used has been limited by resources of a personal computer with 2 Gb RAM and 32 bit operational system. However the new method allowed one to obtain results that are in satisfactory agreement with experimental data and with the calculations performed by industrial FVM (Fine/Hexa by NUMECA Int.) on more dense mesh. Note, that by classification of DPW a mesh with number of cells $1.5 \div 2$ million is considered as coarse one, but even for calculation on such meshes the computer system with greater RAM and 64 bit operational system is required, allowing to work with memory exceeding ~ 3 Gb.
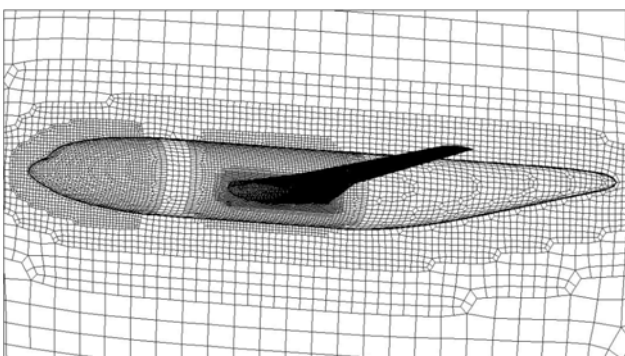

Fig. 6. The fragments of the surface mesh

Mesh #1 for the DLR-F4 configuration, generated by code HEXPRESS™ (NUMECA Int.), contains 229 739 cells. Fragments of a surface mesh on body and wing are represented in Fig. 6. The mean aerodynamic chord of a wing of the configuration is 0.1412 m., length of a fuselage is 1.92 m., and half wingspan is

0.5856 m. The external boundary is represented by a half cylinder with radius of 5 m. and the length 20 m. The cells adjoining to the solid surface has the additional splitting consisting of 4 layers. The distance from the surface to the first layer of nodes is $2 \cdot 10^{-5}$ m., and thickness of the subsequent layers increases with factor of a geometrical series of 1.4.

Calculations are performed at M=0.75 and Re=$3 \cdot 10^6$. The initial factor of turbulent viscosity at infinity in the Spallart-Almaras turbulence model was equal to 5. Comparisons of calculated and experimental pressure distributions in different sections of a wing at zero angle of attack are presented in Fig. 7.

FVM calculations have been performed by on a mesh #2 containing more than 1 million cells. The number of layers in boundary cells of the used mesh was equal to 12, and a factor of a geometrical series was 1.22. Comparisons of calculations results obtained by DGM on a mesh #1 and FVM on a mesh #2 are presented in Fig. 7 and in the table 2. It can be seen that DGM results are in the best agreement with experimental ones [16].
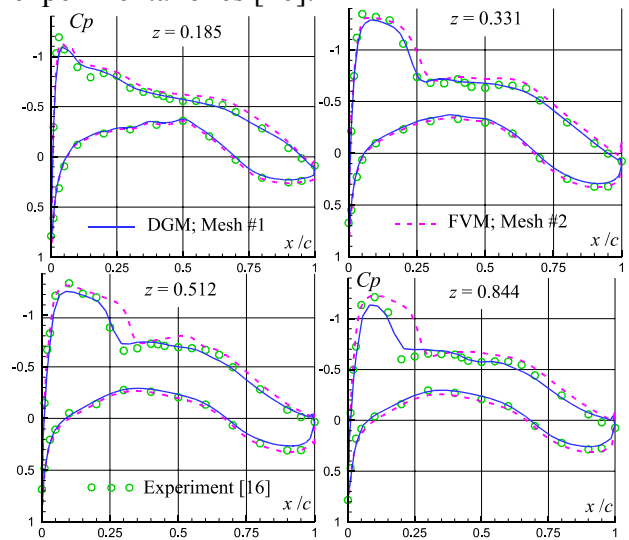

Fig. 7. Comparisons of pressure distributions in different sections of the wing

Table2. Comparison of lift and drag characteristics at α=0

	CL	CD
FVM, mesh #2, 1 mln. cells	0.5728	0.0325
DGM, mesh #1, 230 000 cells	0.4773	0.0303
Experiment [14]	0.4812	0.0278

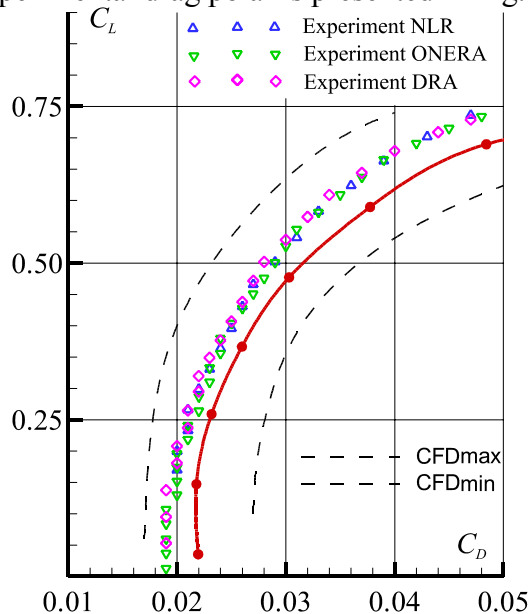Comparison of calculated (DGM) and experimental drag polar is presented in Fig. 8.

Fig. 8. Comparisons of drag polar of the DLR-F4 wing-body configuration

The solid red line correspond to the results of calculation, and markers represent experimental values [16], obtained in various wind tunnels (DLR, ONERA, DRA). Dashed lines limit area of results obtained by various modern FVM presented in materials of DPW conference [17]. The deviation of calculated polar from experimental one is $2 \cdot 10^{-3}$. This deviation is minimal among other results obtained by FVM on meshes with a larger number of cells and with use of greater computer resources.

The analysis of calculations for the given configuration at zero angle of attack, performed by different researchers, shows presence of a separation bubble in the region of aft wing – fuselage junction (Fig. 9). The calculations performed in the present work with DGM even on extremely coarse mesh, confirms this effect.
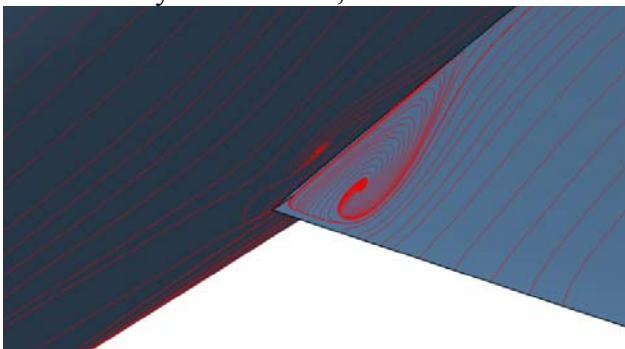

Fig. 9 Separation bubble in the region of aft wing – fuselage junction

Conclusions

The DGM provides accurate results even on coarse grids, when coupled with p-adaptation and anisotropic adaptive meshes. These approaches can significantly reduce computer resources in comparison with the standard finite-volume approach. Meanwhile, the most advantages from DGM application could be reached with high order of accuracy calculations ($K \geq 3$). That will be one of the targets of future work.

References

[1] N.B.Petrovskaya, A.V.Wolkov. The Issues of Solution Approximation in Higher Order Schemes on Distorted Grids. *International Journal of Computational Methods*, Vol. 4, No. 2, pp: 367 – 382, 2007.

[2] Reed W.H. and Hill T.R. (1973) Triangular mesh methods for the neutron transport equation. *Technical Report LA-UR-73-479*. Los Alamos Scientific Laboratory, 1973.

[3] Saint P. Le, Raviart P. On a finite element method for solving the neutron transport equation in: C. de Boor (Ed.), *Mathematical Aspects of Finite Elements in Partial Differential Equations*, Academic Press, New York, pp. 89–145, 1974.

[4] Bassi F. and Rebay S. High-Order Accurate Discontinuous Finite Element Solution of the 2D Euler Equations. *J. Comput. Phys.*, Vol. 138, pp. 251–285, 1997.

[5] Bassi F., Rebay S. A High-Order Accurate Discontinuous Finite Element Method for the Numerical Solution of the Compressible Navier-Stokes Equations. *Journal of Computational Physics* Vol.131, pp. 267-279, 1997.

[6] Cockburn B., Shu C-W. The Local Discontinuous Galerkin Finite Element Method for Convection-Diffusion Systems. *SIAM J. Numer. Anal.*, Vol.175, pp. 2440-2463, 1998.

[7] Cockburn B., Shu C-W. Runge–Kutta Discontinuous Galerkin Methods for Convection-Dominated Problems. *Journal of Scientific Computing*, Vol. 16, No.3, September, 2001.

[8] Shu C.W. Different Formulations of the Discontinuous Galerkin Method for the Viscous Term. *Advances in Scientific Computing*, 2001.

[9] Bassi F, Crivellini A, Rebay S., Savini M. Discontinuous Galerkin solution of the Reynolds-averaged Navier–Stokes and k–ω turbulence model equations. *Computers & Fluids*, Vol. 34, pp. 507–540, 2005.

[10] Wolkov A.V., Lyapunov S.V. Investigation of the Efficiency of Using Numerical Schemes of a High Order of Accuracy for Solving Navier-Stokes and Reynolds Equations on Unstructured Adapted Grids.

Computational Mathematics and Mathematical Physics, Vol. 46, No. 10, pp. 1808-1820, 2006.

[11] Wolkov A.V. Application of the Multigrid Approach for Solving 3D Navier–Stokes Equations on Hexahedral Grids Using the Discontinuous Galerkin Method. *Computational Mathematics and Mathematical Physics*, Vol. 50, No. 3, pp. 495–508, 2010.

[12] Atkins H.L., Shu C.W. Quadrature - Free Implementation of Discontinuous Galerkin Method for Hyperbolic Equations. *AIAA paper* 96-1683，1996.

[13] Cook P.H., McDonald M.A., & Firmin M.C.P. Aerofoil RAE 2822 – pressure distribution, and boundary layer and wake measurements. *AGARD-AR*-138, 1979.

[14] Martynov A.A. Medvedev S.Yu.. A Robust Method of Anisotropic Grid Generator. *Workshop Grid Generatio*n: Theory and Applications Moscow, 2002, Computing Center Russian Academy of Sciences, http://www.ccas.ru/gridgen/ggta02/.index.html.

[15] Chin V.D., Peters D.W., Spaid F.W., and McGhee R.J. Flowfield Measurements about a Multi-Element Airfoil at High Reynolds Numbers. *AIAA-paper-93-3137*, 1993.

[16] Redeker G. DLR-F4 wing body configuration. A selection of experimental test cases for the validation of CFD code. *AGARD-AR-303*, Vol.2., 1994.

[14] Lee-Rausch E., M. Buning P. G., Morrison J. H., Park M. A., Rivers S. M., Rumsey C. L. CFD Sensitivity Analysis of a Drag Prediction Workshop Wing/Body Transport Configuration *AIAA paper* – 3400, 2003.

Contact Author Email Address

andrey.wolkov@mail.ru

Copyright Statement